Ocean Engineering 313 (2024) 119558

Contents lists available at ScienceDirect

Ocean Engineering

journal homepage: www.elsevier.com/locate/oceaneng

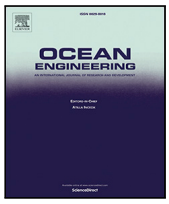

Research paper

Theoretical approximation of gelling concentration: Application to the characterization of consolidation processes in coastal sediment environments

Keivan Kaveh *, Andreas Malcherek

Department of Hydrodynamics and Hydraulic Engineering, Universität der Bundeswehr München, Werner-Heisenberg-Weg 39, Neubiberg, 85577, Bavaria, Germany

ARTICLE INFO

Keywords:
Rheology
Sediment suspension
Gel-like concentration
Consolidation modeling

ABSTRACT

This paper presents a theoretical framework for approximating the gelling concentration in suspensions, with a focus on its application to the parameterization of soil consolidation processes in coastal sediment environments. The model is based on the integration of principles from rheology, colloid science and sedimentology, and the analysis of the change in rheological viscosity as a function of volumetric sediment concentration. Validation is performed against measured rheological data and shows that the model is able to accurately approximate the gelling concentration of sediment under varying environmental conditions. The model provides valuable insights into the consolidation dynamics of saturated soils in estuaries by linking micro-scale sediment properties and macro-scale geotechnical phenomena. In addition, a more robust constitutive equation for estimating effective stress was developed that accounts for both permeability and effective stress regimes by incorporating the underlying physics of each. The results show that the proposed model closely aligns with the conceptual model of sediment concentration profile, accurately depicting the transition from fluid mud to consolidated bed, and capturing the irregularities and inflection points in sediment concentration that were not represented in previous models.

1. Introduction

Gelation is a process that is of importance to wide range of applications in food, pharmaceutical, material and environmental science. Accurate prediction of gelling concentration is a key factor affecting the quality, efficiency and sustainability of industrial processes in many sectors. It enables better control of product characteristics, cost savings, regulatory compliance and environmental benefits. In coastal and marine science, the correct approximation of the gelling concentration c_{gel} (or solids volume concentration at the gelling point $\phi_{s,gel}$) is crucial for modeling sediment transport and deposition patterns, and for informing dredging operations. Knowing the concentration at which sediments consolidate can help optimize dredging schedules and techniques, ensure that navigation channels remain clear, and minimize the frequency and cost of dredging activities. Due to the important role that the gelling concentration c_{gel} plays as the beginning of the consolidation of cohesive sediments and as the transition point from sedimentation to consolidation phase, its estimation, although difficult, seems to be fundamental. It seems, however, that many unknowns still exist about the behavior of a mud suspension at the onset of its gelling concentration (defined as the concentration for which the flocs form a space-filling network Winterwerp and Van Kesteren, 2004). Excessive mud and siltation in estuaries and waterways poses significant challenges to water quality and navigation. High concentrations of suspended sediment block light penetration and reduce photosynthesis in submerged macroalgae, which leads to decreased dissolved oxygen levels and impacts the vitality of aquatic life. Maintaining the required depth in harbors and waterways for navigation and to meet water quality objectives in estuaries requires continuous dredging.

In general, a sedimentation-consolidation process might be represented by three main regimes (Dankers and Winterwerp, 2007). Fig. 1 shows schematic view of these main regimes based on the relation between sediment flux and concentration (see e.g. Dankers and Winterwerp (2007), Kynch (1952) and Camenen and van Bang (2011)). When mud enters calmer waters, sediment particles begin to settle according to Stokes' law. Non-cohesive particles, which contain a significant proportion of clay minerals, can increase in size through aggregation, thereby accelerating the settling process. This is known as flocculation and happens when destabilized clay particles, typically with negatively charged faces and positively charged edges, attract each other. In suspensions with high concentrations of clay particles, the proximity of particles leads to a condition known as hindered settling. In this regime, particles cannot settle freely due to the mutual interference among neighboring flocs and particles. The presence of these interactions reduces the settling velocity compared to that of individual particles in

* Corresponding author.
E-mail addresses: keivan.kaveh@unibw.de (K. Kaveh), andreas.malcherek@unibw.de (A. Malcherek).

https://doi.org/10.1016/j.oceaneng.2024.119558
Received 18 July 2024; Received in revised form 10 September 2024; Accepted 18 October 2024
Available online 30 October 2024
0029-8018/© 2024 The Authors. Published by Elsevier Ltd. This is an open access article under the CC BY license (http://creativecommons.org/licenses/by/4.0/).

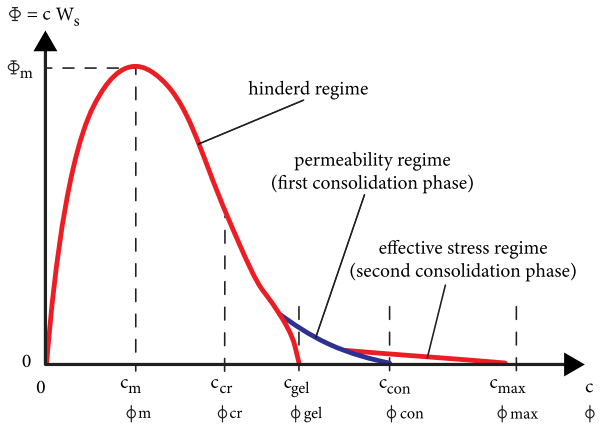

Fig. 1. Schematic view of the three main regimes in a sedimentation-consolidation process based on the relation between sediment flux and concentration (see e.g. Dankers and Winterwerp (2007), Kynch (1952) and Camenen and van Bang (2011)), modified from Camenen and van Bang (2011).

dilute suspensions. As the concentration of solids increases, the settling velocity decreases further. During hindered settling, the descent of the mud-water interface occurs more slowly than during the initial free settling phase. According to Te Slaa et al. (2013), the sedimentation and erosion behavior of silt and silt–clay–sand mixtures is not as well understood compared to that of sand and clay. They noted that in silt–clay–sand mixtures with concentrations exceeding 150–200 g/l, the material undergoes hindered settling, where segregation is either significantly reduced or entirely inhibited.

The end of the hindered settling phase is marked by the attainment of the gelling concentration, which signifies the formation of a space-filling network or "skeleton". At this concentration, all flocs and particles are in continuous contact, preventing any further settling. This gelling concentration represents the transition from hindered settling to the initial phase of consolidation. This transition is characterized by a noticeable decrease in the rate at which the mud-water interface descends. The formation of this network indicates the beginning of the consolidation process, where the sediment bed starts to develop (Meshkati Shahmizadi et al., 2018). This mode physically represents compression and expulsion of pore water (i.e. effective stress $\sigma' \approx 0$). The process continues during the effective stress regime in which sediment particles interconnect and further compression occurs, and finally stops when a certain maximum volume concentration ($\phi_{s,max}$) is attained. This mode represents $\sigma' > 0$ and is normally studied in classical soil mechanics.

Because of the strong differences between these two regimes, the authors prefer not to refer to the permeability regime as a consolidation phase. The permeability regime is dominated by hydraulic processes, while the effective stress regime is dominated by mechanical soil behavior. Lumping them together under the term "consolidation" may obscure these fundamental differences.

Despite the importance of approximating the gelling concentration for various applications ranging from managing suspended sediment concentrations in hyper-turbulent estuaries to processes in chemical engineering, there is currently no comprehensive theoretical model capable of accurately approximating this parameter. As a result, the main objective of this study is to propose a theoretical model to effectively approximate the gelling concentration. The Model is based on the rheological behavior of the suspension. In addition, an attempt is made to extend the proposed framework in such a way as to estimate the concentration level at which the second phase of consolidation begins. The second objective is to apply the proposed model to develop a new parameterization for consolidation of soil in estuarine environments. The advantage of implementing the proposed theoretical model and new parameterization in a hydro-morphodynamic model lies in its ability to improve model consistency, efficiency and accuracy.

2. Definitions, methods and hypotheses

2.1. Rheology of gels

At this point, it is important to clarify the distinction between gels and yielding liquids. The term "gel" is often used in different ways by scientists. By definition, a gel is a non-liquid, soft, elastic substance with a permanent structure. When external forces are applied, gels undergo viscoelastic reversible deformations, but are destroyed once a critical stress state is reached. However, many multicomponent compositions can exist as viscoelastic solids and transition to yielding fluids when an applied load exceeds a certain threshold. These media are often referred to as "gels". This broad use of the term is particularly common in colloidal science, where yielding colloidal substances are typically considered to be gels (Vermonden and Klumperman, 2015). Therefore, a true gel, or solid gel, refers specifically to a non-liquid solid substance. A material that can transition from a solid-like state to a fluid state under external forces is referred to as a "yielding liquid" (or "yield stress" material). These materials may also be called Binghamian liquids or media, in analogy to Newtonian liquids.

The boundary between these states of matter is defined by the yield stress. Below the yield stress, the matter is in a gel-like or solid-like state. Above this threshold, the matter transitions to a liquid or sol state. Traditionally, this transition is referred to in colloidal science as the "sol–gel" or "gel-sol" transition, although it should more accurately be called the gel-like (not gel) to sol transition. This difference in rheological behavior divides gels into chemical gels and physical gels. Chemical gels have permanent covalent bonds, whereas physical gels, such as colloidal gels, have temporary and weak bonds (Zaccarelli, 2007).

Sol–gel transition of physical gels has been studied intensively from mechanistic viewpoints, and several approaches by mechanical, thermal and spectroscopic measurement techniques have been conducted through the dynamic methods. However, it remains difficult to determine the transition temperature or concentration through the dynamic rheological, spectroscopic, or thermal measurements owing to the variation in the definition of gel, which depends on the measurement technique employed (Ichinose and Ura, 2020). The main focus of this study is the sol–gel transition of physical gels, although the presented method may be applied to chemical gels as well.

2.2. Rheological model

In rheology, viscosity is a measure of a fluid's resistance to deformation under shear stress. Under assumption of monodisperse spherical particles and by comparing Casson's rigid rod model (Casson, 1959) with Cross's model (Cross, 1965) of random chain formation in flocculation, (Kaveh and Malcherek, 2024a) proposed a model the rheology of suspensions as

$$\mu_{rh} = \mu_\infty + \underbrace{\left[\frac{1 + \frac{1}{k_0' d_p}\left(\alpha'' \phi_s\right)^{1/2q}}{\hat{d}_{f,eq}}\right]^{n_f}}_{F(\phi_s,\dot{\gamma})} \frac{\mu_0 - \mu_\infty}{1 + \beta\dot{\gamma}^n} \tag{1}$$

where $\dot{\gamma}$ is applied shear rate in reciprocal seconds, ϕ_s is volume fraction of particles in suspension, d_p is particle size, n_f is fractal dimension, k_0', α'' and β are proportionality constants, μ_0 and μ_∞ are viscosity when $\dot{\gamma} = 0$ and $\dot{\gamma} \to \infty$, respectively. The function $F(\phi_s, \dot{\gamma})$ is the extension factor added to the original Cross rheological model (Cross, 1965). The dimensionless equilibrium floc size $\hat{d}_{f,eq}$ in Eq. (1) is defined as

$$\hat{d}_{f,eq} = \frac{d_{f,eq}}{d_p} = 1 + \frac{\left(\alpha'' \phi_s\right)^{1/2q}}{k_0' d_p (1 + \beta' \dot{\gamma}^{0.5})} \tag{2}$$

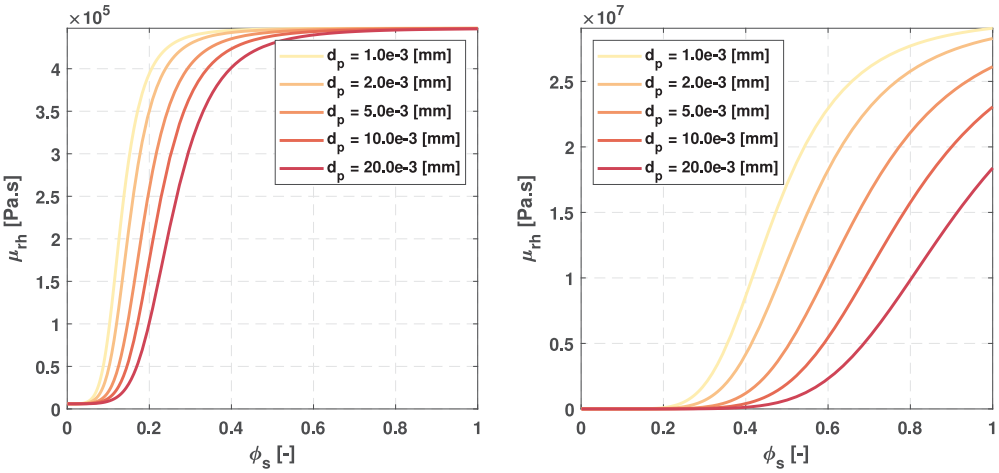

Fig. 2. Change in viscosity with increasing solid volume fraction ϕ_s for different particle sizes at (left) $\dot{\gamma} = 10^{-6}$ [1/s] and (right) $\dot{\gamma} = 10^{-1}$ [1/s].

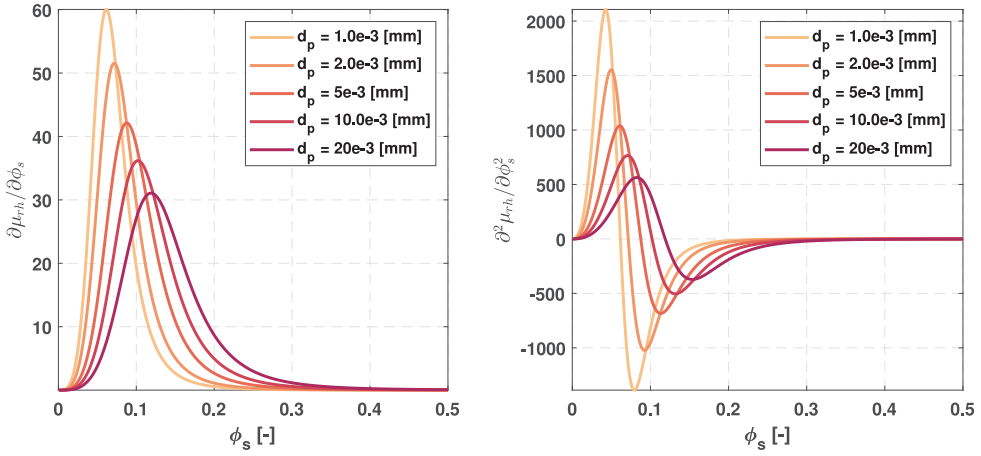

Fig. 3. (left) The first and (right) second derivatives of viscosity with respect to the volumetric sediment fraction for different particle diameters.

The proposed rheological model takes into careful consideration the impact of concentration and sediment size, recognizing that these factors play pivotal roles in shaping the model's outcomes. The equilibrium floc size, which is a fundamental determinant of a suspension's rheological behavior, is intricately tied to these parameters. Concentration affects the extent of particle–particle interactions and the overall density of the suspension, which, in turn, influences floc formation and size. Moreover, sediment size directly influences the agglomeration tendencies and the ease with which particles can form stable flocs (see Kaveh and Malcherek (2024a)).

2.3. Determination of gel-like concentration

The behavior of viscosity with respect to concentration, especially in systems undergoing gelation, can be quite complex. Fig. 2 shows variation of viscosity as a function of the volumetric sediment fraction ϕ_s for different particle diameters d_p based on Eq. (1). Each plot corresponds to a different shear rate $\dot{\gamma}$ value. As can be seen from Fig. 2, a general overview of how rheological viscosity changes with increasing concentration at a fixed shear rate can be divided into three groups: (1) below gelling concentration, (2) at gelling concentration, and (3) above gelling concentration. Before reaching the gelling concentration, the viscosity typically increases with concentration. This is due to the increased interactions between the particles or molecules in the suspension, leading to greater resistance to flow. The gel-like concentration is the point at which a continuous network starts to form throughout the entire system. At this point, there is a dramatic increase in viscosity. The system transitions from a viscous liquid to a viscoelastic gel. The viscosity can become very high if measured over very long timescales, as the system exhibits a solid-like response to deformation. Beyond the gelling concentration, the system behaves as a gel with a densely packed network of particles. The viscosity continues to increase with concentration, but the rate of increase ($\partial\mu_{rh}/\partial c$ or $\partial\mu_{rh}/\partial\phi_s$) can vary depending on the nature of the network and its rigidity. To analyze this, the first derivative of rheological viscosity μ_{rh} in Eq. (1) with respect to solid volume concentration ϕ_s is calculated as

$$\frac{\partial\mu_{rh}}{\partial\phi_s} = \frac{n_f\alpha'' F^{\frac{n_f-1}{n_f}}}{2q}\left(\frac{(A - BF^{\frac{1}{n_f}})(\alpha''\phi_s)^{\frac{1}{2q}-1}}{B(\alpha''\phi_s)^{\frac{1}{2q}}+1}\right)\frac{(\mu_0-\mu_\infty)}{\beta\dot{\gamma}^n+1} \tag{3}$$

where A and B are defined as $A = 1/(k_0' d_p)$ and $B = A/(1+\beta'\dot{\gamma}^{0.5})$, respectively.

Fig. 3 provides insights into the rate of viscosity changes with volumetric sediment concentration for different particle sizes. Each curve exhibits a peak at a certain ϕ_s value, indicating the point where the rate of increase in viscosity with respect to ϕ_s is maximal. This point could be defined as the solids volume concentration at the gelling point $\phi_{s,gel}$, as the proposed hypothesis suggests that a significant change in viscosity occurs at this point. While the viscosity continues to increase beyond this point, the rate of change decreases thereafter. Therefore, the gelling point is defined as the point at which the rate of change of viscosity with respect to solid volume fraction, $\partial\mu_{rh}/\partial\phi_s$, reaches its maximum. The peaks shift to higher ϕ_s values as the particle diameter

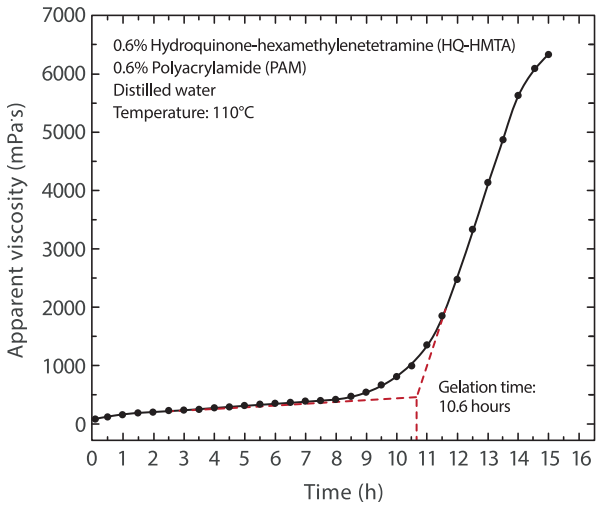

Fig. 4. Determination of the gelation time (Liu et al., 2016).

d_p increases. This suggests that larger particles reach their gel-like state at higher sediment concentration. The points where the second derivatives cross zero correspond to inflection points on the $\partial^2\mu_{rh}/\partial\phi_s^2$ curves, marking transitions between concave and convex regions. Therefore, solving $\partial^2\mu_{rh}/\partial\phi_s^2 = 0$ yields $\phi_{s,gel}$. Since the shear rate becomes very small at gelling concentration, a very small value ($\dot{\gamma} = 1e{-}10$ [1/s]) was chosen for this analysis. The results show that reducing the shear rate further has no effect on the final results. However, according to Kaveh and Malcherek (2024a), it should be noted that the shear rate $\dot{\gamma}$ cannot be set to zero, because in this case the viscosity is no longer a function of the concentration, which is one of the limitations of the rheological model.

In chemical engineering, the gelation time is defined as the time required to reach the inflection point on the apparent viscosity versus time curve, as shown in Fig. 4. The inflection point corresponds to the onset of the gel formation. This method has been widely used to approximate of gelation time (Liu et al., 2016). According to Malkin et al. (2023), the x-axis does not necessarily represent time, but e.g. temperature or a change in the composition of the matrix due to the addition of certain chemicals. With ϕ_s as the x-axis, we apply the same method to the $\mu_{rh} - \phi_s$ plot in Fig. 2 for $d_p = 20$ µm, where the x-axis represents the solids volume concentration instead of time. Similar to Fig. 4, to calculate the inflection point, two tangent lines are plotted so that the intersection of these lines corresponds to the gelling concentration. The results are plotted in Fig. 5 showing that the obtained value is exactly the value obtained by solving $\partial^2\mu_{rh}/\partial\phi_s^2 = 0$. This shows that the hypothesis assumed for calculation of the gel-like concentration is valid. Overall, Fig. 5 illustrates how the proposed method potentially offers a more precise determination of the gelling concentration by focusing on the underlying changes in the viscosity curve's curvature, rather than relying solely on tangent lines.

Fig. 6 shows the variation of $\partial^2\mu_{rh}/\partial\phi_s^2$ with respect to changes in solids volume fraction ϕ_s and shear rate $\dot{\gamma}$ for two different particle sizes. The blue solid lines in the plots correspond to $\partial^2\mu_{rh}/\partial\phi_s^2 = 0$, showing that the volume fraction of gelling solids $\phi_{s,gel}$ increases with increasing shear rate. Moving along the blue solid line, the rate of change in ϕ_s decreases with increasing shear rate. There is a point where increasing the shear rate has no effect on the changes observed in the solids volume fraction. $\phi_{s,con}$ represents a critical solid volume fraction where a notable change in the rheological behavior of the suspension occurs, marking the transition from a gel-like to a solid-like state. In fact, we have assumed that in the second phase of consolidation, the soil-like state is formed which is sufficiently compacted and the concentration has increased to a level where further increases in shear rate have minimal effect on its properties. This assumption is reasonable, as the soil structure is likely to have reached a state of equilibrium at this stage, where the effects of additional shear are significantly reduced. As the soil becomes denser and more consolidated, its rheological behavior stabilizes and becomes less susceptible to changes induced by shear rate variations. This point can be considered the consolidation solids volume fraction $\phi_{s,con}$. According to Fig. 6, the parameter $\phi_{s,con}$ can be estimated by drawing two tangent lines and identifying the point of intersection where a significant shift in the behavior of the system occurs, which is associated with a transition to a continuous solid phase or network formation. In fact, the first tangent line is drawn in the lower ϕ_s region, where the system behaves as a relatively dilute suspension. The second tangent line is drawn in the higher ϕ_s region, where particle interactions are dominant, and the system transitions to a continuous phase.

It can be seen from Fig. 6 that at a constant shear rate (e.g. $\dot{\gamma} = 0.01\ s^{-1}$), the compact concentration of smaller particles occurs at lower concentrations. This phenomenon occurs because larger particles require higher concentrations to generate the same level of frictional forces between them as smaller particles, which have a higher surface area to volume ratio. Consequently, smaller particles achieve their compact state at lower concentrations than larger particles.

3. Application for consolidation modeling

3.1. Governing equations

Consolidation begins in the permeability regime particularly when the gelling volume concentration $\phi_{s,gel}$ is reached. This process continues into the effective stress regime, where sediment particles aggregate and undergo further compression, and finally stops when a certain maximum concentration $\phi_{s,max}$ is reached (Zhou et al., 2016). In this study, we apply a modified form of Gibson-type consolidation model (Gibson et al., 1967), which is formulated with solids volume concentrations as time-dependent variable in a Eulerian coordinate system as (Schmidt and Malcherek, 2021)

$$\frac{\partial\phi_s}{\partial t} + \frac{\partial}{\partial z}\left[\underbrace{k_f\phi_s(1-\phi_s)(1-\frac{\rho_s}{\rho_w})}_{W_c}\phi_s\right] = \frac{\partial}{\partial z}\left[\frac{k_f(1-\phi_s)\phi_s}{g\rho_w}\frac{\partial\sigma'}{\partial z}\right] \tag{4}$$

where W_c is consolidation settling velocity, σ' is the effective stress, k_f is soil permeability, ρ_w is density of water, ρ_s is density of sediment, z is vertical coordinate and t is time. To solve Eq. (4), it is necessary to introduce two constitutive closure equations for predicting soil permeability k_f and effective stress σ'. In this research we apply the Kozeny–Carman equation (Kozeny, 1927; Carman, 1939) for calculation of soil permeability as

$$k_f = c_1\frac{g d_{10}^2}{\nu}\frac{(1-\phi_s)^3}{\phi_s^2} \tag{5}$$

where ν is kinematic viscosity of water, d_{10} is diameters corresponding to 10% passing in grain size distribution and c_1 is proportionality constant. The parameterization of effective stress is presented in the following section.

3.2. Analyzing previous parametrizations for effective stress

Different formulations are considered for parameterizing effective stress. Merckelbach (2000) proposed the effective stress closure as

$$\sigma' = A_\sigma\phi_s^{B_\sigma} - C_\sigma \tag{6}$$

where $3.9\times10^8 \le A_\sigma \le 4.1\times10^9$ Pa, and $7.1 \le B_\sigma \le 8.0$ and C_σ are proportionality constants.

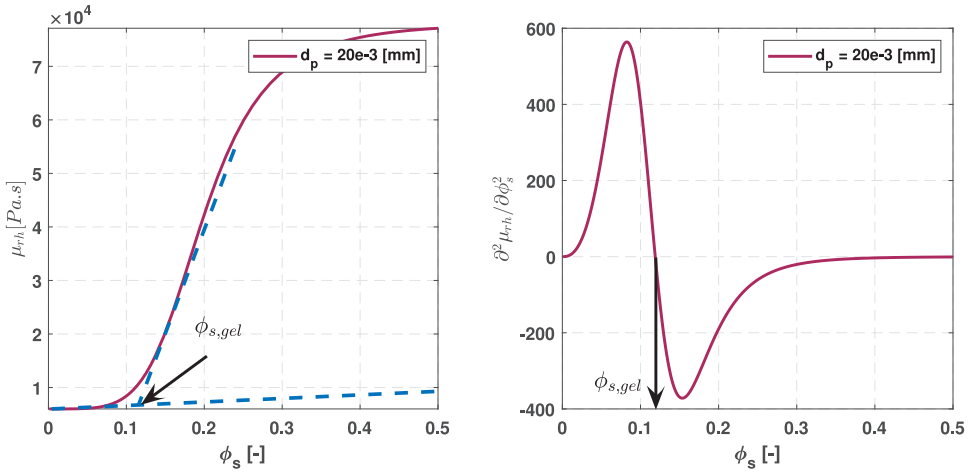

Fig. 5. Comparison between determination of the gelling concentration using tangent lines and the proposed method.

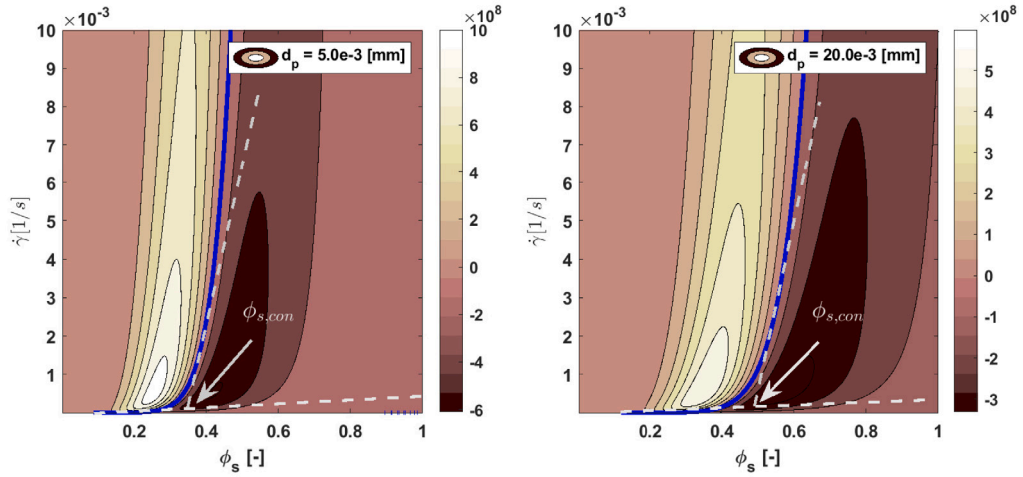

Fig. 6. Response of the second derivative of viscosity with respect to solids volume concentration ($\partial^2\mu_{rh}/\partial\phi_s^2$) to increasing shear rate and solids volume concentration for two particle diameters d_p.

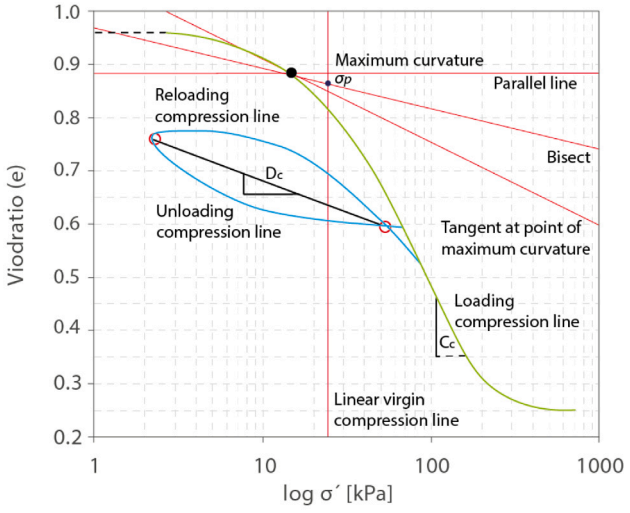

Fig. 7. Compressibility of soil describing consolidation characteristics of normally consolidated soil according to classical soil mechanics.

Using an experimental settling column of nearly 10 m, Townsend and McVay (1990) investigated various soil consolidation processes induced by either the soil's self-weight or external loading. Their study focuses solely on the self-weight consolidation experiment (scenario A from Townsend and McVay (1990)). The sediment used was drained clay with an initial uniform volume fraction $\phi_{s,0}$ of 0.0633 (corresponding to a sediment concentration of 167.7 kg/m^3). The constitutive equation describing the effective stress can generally be expressed as follows:

$$\sigma' = (\frac{b}{e})^n + \sigma_0' \tag{7}$$

where $e = (1/\phi_s) - 1$ is the soil void ratio and b, n and σ_0' are proportionality constants set to 7.22, 1/0.22 and 0, respectively.

By considering modulus of volume change and assuming the linear relationship between the change in volume of voids and the effective stress, Kaveh and Malcherek (2024b) developed a relationship between the soil permeability k_f and the effective stress σ' as

$$\sigma' = -\frac{1}{a}(k_f - k_{f0}) + \sigma_0' \tag{8}$$

where k_f can be calculated using Eq. (5), k_{f0} is the point function for the soil permeability and a and σ_0' are proportionality constants.

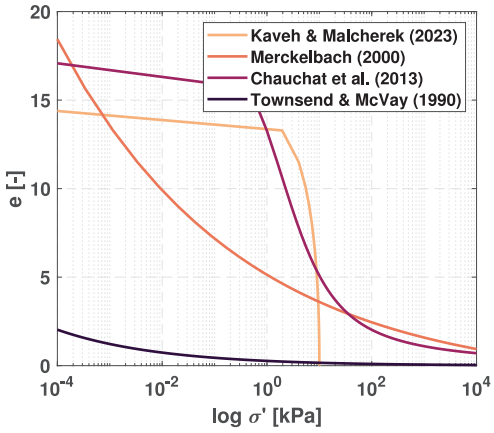

Fig. 8. Compressibility of soil describing consolidation characteristics of normally consolidated soil according to different parameterizations.

The following effective stress closure was introduced by (Chauchat et al., 2013)

$$\sigma' = \begin{cases} 0, & \text{if } \phi_s \le \phi_{s,gel} \\ \sigma_0'' \left[\left(1 - \frac{\phi_{mud} - \phi_{s,gel}}{\phi_{s,max}} \right)^{-n} - 1 \right], & \text{if } \phi_s > \phi_{s,gel} \end{cases} \tag{9}$$

where σ_0'' is the effective stress modulus (Pa), ϕ_{mud} is solids volume concentration of mud and $\phi_{s,max}$ is the maximum solids volume concentration. Both parameters should be determined by laboratory or field experiments.

In order to evaluate the above parameterizations, it is necessary to correctly analyze typical soil compressibility. Fig. 7 shows a typical soil compressibility where the effective stress is on the horizontal axis in logarithmic scale and the void ratio is on the vertical axis. In general, soils exhibit two types of behavior depending on their previous consolidation state. Normal consolidation occurs when the soil consolidates under the weight of the overlying soil layers. The soil has not previously been subjected to pressures greater than the current effective stress, i.e. it is experiencing its maximum historical pressure. Self-weight consolidation is a typical condition of normal consolidation. Overconsolidation occurs when the soil has previously been subjected to a higher effective stress than it is currently experiencing. Overconsolidated soils have already been compacted under pressures greater than their current load, often due to historical geologic processes or human activities such as excavation and loading/unloading. An important point that should be taken into account is that Fig. 7 describes compressibility of soil under the effective stress regime (i.e. $e \approx 1.0$ or $\phi_s \approx 0.5$) based on classical soil mechanics. In other word, this plot is valid only for $\phi_{s,con} < \phi_s \le \phi_{s,max}$. Comparing Fig. 8 which illustrates the compressibility of soil based on different parameterizations, with Fig. 7 suggests that parameterizations proposed by Chauchat et al. (2013) and Kaveh and Malcherek (2024b) provide a more realistic representation of soil compressibility. They align well with the general trends observed in soil behavior, while model proposed by Chauchat et al. (2013) showing better agreement and therefore can be considered more robust for predicting soil compressibility. However, it should be noted that the expected behavior should be in the range of $e \approx 0.15$–1.0 or $\phi_s \approx 0.5$–0.85. Although a consolidation test should be performed on a specific sample under investigation to determine the exact soil compression, these values can be considered as an acceptable approximation. For example, Urmi and Ansary (2019) performed a one dimensional consolidation test on the soil samples collected from 17 different locations of coastal embankments. Their results show that the initial void ratio for undisturbed samples at depth of 2.10–4.05 m were in the range of 0.796–0.567.

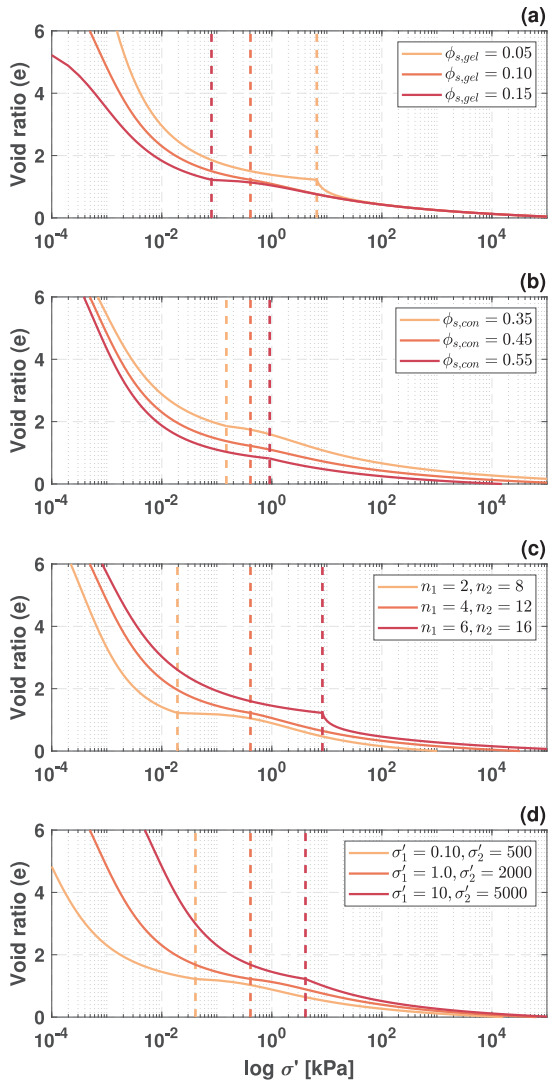

Fig. 9. Parameterization of soil compressibility according to the proposed parameterization Eq. (10) for different variables. The dashed line separates the permeability and the effective stress regimes into the left and right parts, respectively. Other constants are (a) $\phi_{s,con} = 0.45$, $\phi_{s,max} = 0.95$, $\sigma_1'' = 1$, $\sigma_2'' = 1000$, $n_1 = 4$, $n_2 = 15$ and (b) $\phi_{s,gel} = 0.01$, $\phi_{s,max} = 0.95$, $\sigma_1'' = 1$, $\sigma_2'' = 1000$, $n_1 = 4$, $n_2 = 15$ and (c) $\phi_{s,gel} = 0.10$, $\phi_{s,con} = 0.45$, $\phi_{s,max} = 0.95$, $\sigma_1'' = 1$, $\sigma_2'' = 1000$, $n_1 = 4$, $n_2 = 15$ and (d) $\phi_{s,gel} = 0.10$, $\phi_{s,con} = 0.45$, $\phi_{s,max} = 0.95$, $n_1 = 4$ and $n_2 = 12$.

Table 1 presents some index and engineering properties of marine sediments, with most data limited to the upper 2 m of the seafloor (Thompson et al., 2012). According to this table γ_b is the buoyant unit weight of soil, w_n is the natural water content, w_p is the plastic limit, and w_l is the liquid limit. As can be seen, the averaged buoyant unit weight for clayey silt is about 15 kN/m^3, which corresponds to a void ratio of about 2.1. This value is much lower (about less than 1.0) for sandy clayey silt.

Most importantly, all parameterizations show high values for the effective stress in the permeability regime (e.g. $e > 1.5$), which is not correct since the effective stress is assumed to be very small in this regime. According to Gibson et al. (1981), who studied consolidation of a soft homogeneous soil layer for Osaka Harbor mud, a void ratio of 4.0 corresponds to an effective stress of 0.1 kPa. Although this value may be different for another soil under different conditions, it can be used as a reference. This discrepancy is due to the fact that the proposed model of Chauchat et al. (2013) does not distinguish between the permeability regime and the effective stress regime.

Table 1
Some index and engineering properties of ocean sediments (Thompson et al., 2012).

Type		Water depth	w_n%	w_l	w_p	CaCO3%	γ_b [kN/m^3]
Pelagic	Calcareous ooze	3.16	86–116	43	–	88	13.8–15.4
	Calcareous ooze	3.53	156–212	–	–	72–77	12.6–13.1
	Calcareous ooze	4.10	112–248	–	–	68–81	12.4–14.0
	Calcareous ooze	4.3	102–196	–	–	70–87	12.8–14.3
Siliceous ooze	Clayey Diatom Ooze (1.2–10 m)	2.649	151	71	47	Small	13.0–14.0
	Silt rich Diatom ooze (230 m)	2.649	119	–	–	Small	13.0–13.5
	Diatom ooze (118 m)	2.414	87–106	–	–	1	13.8–13.9
Pelagic clay	Pelagic clay (Abyssal hills)	5.421	112–138	91–103	35–38	0.1	14.1
	Iron oxide (Abyssal hills)	5.163	202–235	225–229	97–101	0	13.0
Terrigenous	Terrigenous Clayey Silt	180	44–59	35–48	29–32	Negligible	16.6–17.8
	Terrigenous Clayey Silt (basin)	370	73–108	73–88	43–49	Negligible	14.4–15.4
	Terrigenous Clayey Silt	1700	104–144	109–121	61–89	Negligible	13.5–14.3

3.3. Proposed parameterization for effective stress

In a coastal and estuarine environment with a long-established soil layer covered by a potentially dynamic mud layer, the density profile of the combined soil-mud system will exhibit distinct characteristics due to the differing physical properties and behaviors of the two layers. Just above the boundary with the soil layer, the mud will be more compacted and thus denser than at the surface, but still generally less dense than the underlying soil.

To create a more robust parameterization that clearly accounts for both the permeability and effective stress regimes, we can create separate models for each regime and then integrate these model appropriately as

$$\sigma' = \begin{cases} 0, & \text{if } \phi_s < \phi_{s,gel} \\ \sigma_1'' \left[\left(1 - \frac{\phi_s - \phi_{s,gel}}{\phi_{s,con}} \right)^{-n1} - 1 \right], & \text{if } \phi_{s,gel} \le \phi_s < \phi_{s,con} \\ \sigma_2'' \left[\left(1 - \frac{\phi_s - \phi_{s,con}}{\phi_{s,max}} \right)^{-n2} - 1 \right] + \sigma_{2,0}'', & \text{if } \phi_{s,con} \le \phi_s < \phi_{s,max} \end{cases} \tag{10}$$

where σ_1'' and σ_2'' are the effective stress modulus (Pa) and $\sigma_{2,0}''$ is defined as

$$\sigma_{2,0}'' = \sigma_1'' \left[\left(1 - \frac{\phi_{s,con} - \phi_{s,gel}}{\phi_{s,con}} \right)^{-n1} - 1 \right] \tag{11}$$

Fig. 9 illustrates the compressibility of soil according to the new proposed parameterization for a wide range of parameters. As can be seen from this figure, the curve is divided into two distinct phases: the first and the second consolidation phases. The dashed lines separating the two phases are at the position where the first phase ends and the second phase begins. This corresponds to the value of $\sigma_{2,0}''$ in Eq. (11). In the first phase, the left side of the dashed line, the void ratio decreases rapidly from approximately 5 to around 1 as the effective stress increases from 10^{-5} kPa to around 10^{-1} kPa. This phase indicates a significant reduction in void spaces within the soil, likely due to the initial loading. Most importantly, during this phase, the effective stress is very small, confirming that the new parameterization is in better agreement with the physics of the permeability regime where the effective stress is almost zero. The second consolidation phase, the right side of the dashed line, shows a more gradual decrease in the void ratio from about 1 to nearly 0 as the effective stress continues to increase up to 10^5 kPa. This phase suggests a continued, but less pronounced, compression of the soil as it undergoes further loading. The overall behavior depicted in the graph is typical of soil undergoing consolidation under increasing effective stress, where the void ratio decreases as the particles pack more tightly together.

By determining the dominant regime based on the solids volume concentration and right estimations of $\phi_{s,gel}$ and $\phi_{s,con}$ (Section 2.3), the model appropriately applies the correct parameterization for the current soil state. This ensures that both permeability and effective stress influences are considered accurately.

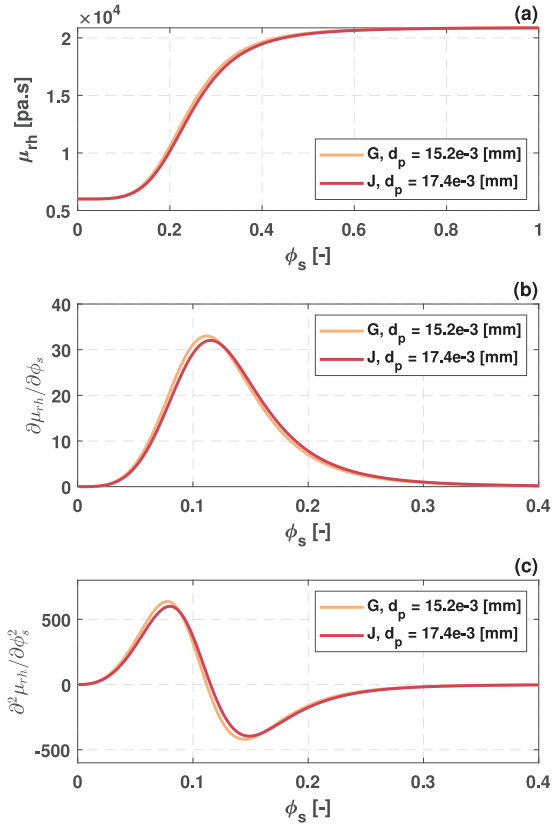

Fig. 10. (a) Change in viscosity with increasing solid volume fraction ϕ_s for samples G and J according to Eq. (1) based on the calibrations values obtained by Kaveh and Malcherek (2024a); (b) the first and (c) the second derivatives of viscosity with respect to the volumetric sediment concentration for samples G and J.

3.4. Proposed parameterization for vertical consolidation rate

As mentioned above, researchers typically combine the permeability regime with the effective stress regime and use a single model for both regimes, even though the underlying physics of these regimes are completely different. This is not only the case for the effective stress σ' constitutive equation, but also for the vertical consolidation rate. An example is Eq. (12) which is introduced by Camenen and van Bang (2011) and rewritten by Zhou et al. (2016) as

$$W_s = \begin{cases} W_h, & \text{if } \phi_s \le \frac{\phi_{s,gel}}{\chi} \\ W_h^{gel} \left(\frac{\chi \phi_{mud}}{\phi_{s,gel}} \right)^{1-n}, & \text{if } \phi_s > \frac{\phi_{s,gel}}{\chi} \end{cases} \tag{12}$$

where W_h is hindered settling, χ is considered as a transition point to distinguish between sedimentation and consolidation (where $\chi > 1.0$)

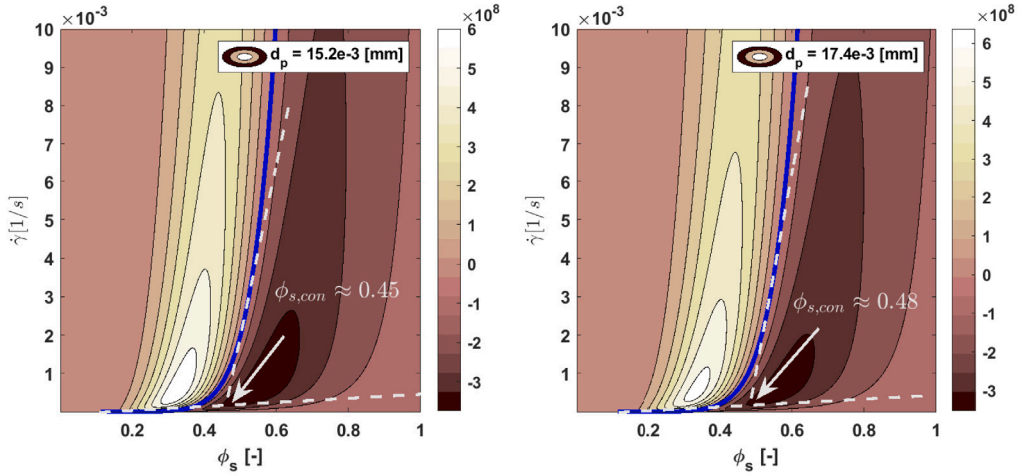

Fig. 11. Response of the second derivative of viscosity with respect to solids volume concentration ($\partial^2\mu_{rh}/\partial\phi_s^2$) to increasing shear rate and solids volume concentration for samples G (d_p = 15.2 μm) and J (d_p = 17.4 μm).

and W_h^{gel} corresponds to the value oh W_h at $\phi_{mud} = \phi_{s,gel}/\chi$. The parameter χ is considered to ensure the identical slope (hence continuity) of settling velocities between the permeability and consolidation regimes.

As can be seen from Eq. (12), a single relation is used for both the permeability and effective stress regimes for $\phi_s > \phi_{s,gel}/\chi$. In order to distinguish between the consolidation rate in the two regimes, a new consolidation rate is applied in Eq. (13) to create a transition from hindered settlement to consolidation rate during the permeability regime. According to Kaveh and Malcherek (2024b), the rheological viscosity μ_{rh} can be considered as the effective viscosity for modeling hindered settling from low to high concentrations. This idea has been successfully applied to the parameterization of a 1D vertical (1DV) hydromorphodynamic model of estuaries (Kaveh and Malcherek, 2024b). Here we replace the rheological viscosity by Eq. (1) and calculate the consolidation rate for the permeability regime as

$$W_s = \begin{cases} \frac{\mu}{\mu_{rh}} W_{s0}, & \text{if } \phi_s < \phi_{s,gel} \\ \frac{\mu}{\mu_{rh}} W_{s0}, & \text{if } \phi_{s,gel} \le \phi_s < \phi_{s,con} \\ W_c, & \text{if } \phi_{s,con} \le \phi_s < \phi_{s,max} \end{cases} \tag{13}$$

where μ is viscosity of fluid so that $\mu/\mu_{rh} < 1.0$ and W_{s0} is Stokes' settling velocity. For a single, spherical particle with diameter d_p, it can be expressed as

$$W_{s0} = \frac{1}{18}\frac{g d_p^2}{\mu}(\rho_w - \rho_s) \tag{14}$$

where μ is dynamic viscosity of water.

4. Results and discussion

4.1. Case study and estimation of $\phi_{s,gel}$ and $\phi_{s,con}$

In order to apply the proposed parameterization for the calculation of the consolidation process, the values of $\phi_{s,gel}$ and $\phi_{s,con}$ must first be determined. This requires rheological experiments on the case study samples to calibrate Eq. (1) and find the proportionality constants k_0', q, α'', β, β', n, and n_f. We used the experiments reported by Kaveh and Malcherek (2024a) on two samples from the Ems estuary at two different locations, Gandersum (sample G) and Jemgum (sample J). The grain size distributions for these samples showed similar grading curves with mean diameters of $d_{p,G}$ = 15.2 μm and $d_{p,J}$ = 17.4 μm. The initial solid content was $\phi_s = 0.2$, and solid fractions of $\phi_s = 0.16$, 0.13, 0.10 and 0.07 were produced. Rheometer rotation tests were then performed under controlled shear stress according to a specific protocol until a shear rate of 100 s^{-1} was reached. The measured data were used to calibrate the model. The calibration process is discussed in detail in Kaveh and Malcherek (2024a). Fig. 10 illustrates the change in viscosity using the obtained calibrated parameters for samples G and J. To obtain an approximation for $\phi_{s,gel}$ and $\phi_{s,con}$, the first and second derivatives of viscosity with respect to solids volume concentrations are calculated for both samples and are plotted in Fig. 10. Since both samples have nearly identical grain size distributions, the calculated $\phi_{s,gel}$ values are very similar: 0.112 and 0.115 for samples G and J, respectively. Fig. 11 illustrates the changes in viscosity with increasing shear rate, showing that $\phi_{s,con}$ for the samples G and J is approximately 0.45 and 0.48, respectively. Due to the similarity of the two samples, only one of them, sample G, is used for analysis in this research.

4.2. Consolidation model development

For modeling of self-weight consolidation behavior, the chain rule can be applied to calculate derivative of Eq. (10) with respect to z as

$$\frac{\partial\sigma'}{\partial z} = \begin{cases} 0, & \text{if } \phi_s < \phi_{s,gel} \\ \frac{n_1\sigma_1''}{\phi_{s,con}}\left(1 - \frac{\phi_s - \phi_{s,gel}}{\phi_{s,con}}\right)^{-n_1-1}\frac{\partial\phi_s}{\partial z}, & \text{if } \phi_{s,gel} \le \phi_s < \phi_{s,con} \\ \frac{n_2\sigma_2''}{\phi_{s,max}}\left(1 - \frac{\phi_s - \phi_{s,con}}{\phi_{s,max}}\right)^{-n_2-1}\frac{\partial\phi_s}{\partial z}, & \text{if } \phi_{s,con} \le \phi_s < \phi_{s,max} \end{cases} \tag{15}$$

Replacing Eqs. (15) and (5) into Eq. (4), the new form of Gibson's equation can be modeled as a 1DV advection–diffusion partial differential equation (PDE). The equation is formulated in finite volume method and solved with an implicit numerical scheme.

In order to apply the initial condition for calculating the new form of Gibson's equation, we apply the stationary solution of it using Eq. (10). Setting $\partial\phi_s/\partial t = 0$ results in

$$\frac{\partial\phi_s}{\partial z} = \begin{cases} \frac{g(\rho_w - \rho_s)\phi_{s,con}}{n_1\sigma_1''}\phi_s\left[1 - \frac{\phi_s - \phi_{s,gel}}{\phi_{s,con}}\right]^{n_1+1}, & \text{if } \phi_{s,gel} \le \phi_s < \phi_{s,con} \\ \frac{g(\rho_w - \rho_s)\phi_{s,max}}{n_2\sigma_2''}\phi_s\left[1 - \frac{\phi_s - \phi_{s,con}}{\phi_{s,max}}\right]^{n_2+1}, & \text{if } \phi_{s,con} \le \phi_s < \phi_{s,max} \end{cases} \tag{16}$$

Specifically, the Eq. (16) is solved using the fourth-order Runge–Kutta method, a robust and widely-used numerical technique for solving ordinary differential equations (ODEs). A 9-day simulation using new parameterization is then performed to establish an initial condition characterized by the formation of a two-layer soil structure.

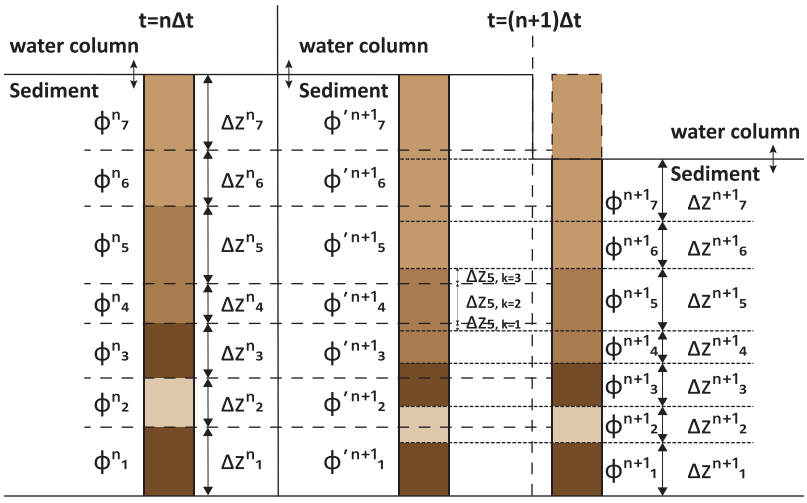

Fig. 12. Cell size adjustment from time step n to time step $n+1$ via interpolated porosity distribution.

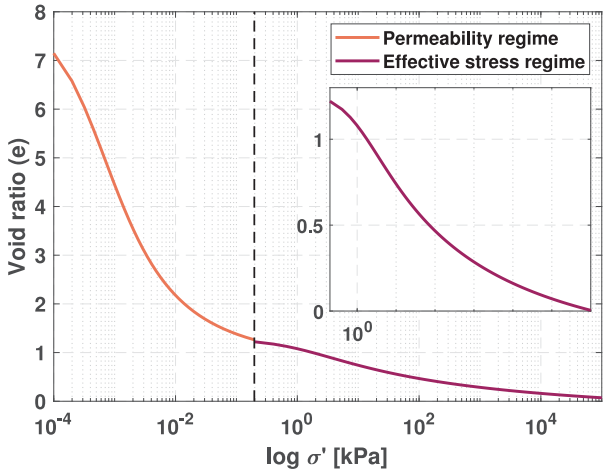

Fig. 13. Parameterized compressibility of soil for the sample G.

4.3. Cell size adjustment

The dependent quantity ϕ_s is calculated at each time step and the thickness of each cell is updated accordingly. The main context of adjusting cell size is based on conservation of mass M_S. At a given time step n, cell i forms layer l, and the mass in that layer remains constant from time step n to the next $(n+1)$. Mathematically, this is expressed as

$$M_{S,i} = \rho_s \phi^n_{s,i} \Delta z^n_i = \rho_s \phi^{n+1}_{s,i} \Delta z^{n+1}_i \tag{17}$$

Consequently, a layer has a time-independent solid mass $M_{S,l}$. This allows us to determine a new cell height Δz_i at a later time step based on a changed concentration as

$$\Delta z^{n+1}_i = \frac{M_{S,l}}{\rho_s \phi^{n+1}_{s,i}} \tag{18}$$

The challenge lies in determining ϕ_s at the new time step, which requires a more precise definition of the relationship between layer, concentration, and cell. During consolidation, an overlying layer moves across its cell boundaries into the cell below. Although the concentration was initially calculated using the transport equation based on the lattice structure, a direct link between the determined concentration and the layer is lost. This complicates the determination of the new layer-bound cell height. To address this issue, we introduce the concept of cell-bound and layer-bound concentrations, denoted ϕ'_s and ϕ_s, respectively.

An intermediate step is introduced (shown in Fig. 12) to determine the relationship between the cell height Δz^n_i from the old time step n and a cell-bound concentration $\phi'^{n+1}_{s,i}$ at the new time step $n+1$. The new cell- and layer-bound concentration at time $n+1$ is obtained from a weighted average of the cell-bound concentrations, where the weight is the fraction of the considered layer as

$$\phi^{n+1}_{s,i} = \frac{\sum_{k=1}^{N_k} \phi'^{n+1}_{s,k} \Delta z^n_{l,k}}{\sum_{k=1}^{N_k} \Delta z^n_{l,k}} \tag{19}$$

Here, k represents the cells over which the layer l is distributed, and $\Delta z_{l,k}$ is a proportional cell height of the examined cell. This process involves an iterative adjustment of cell heights until equilibrium is reached as

$$\phi^{n+1}_{s,i} \Delta z^{n+1}_i = \sum_{k=1}^{N_k} \phi'^{n+1}_{s,k} \Delta z^n_{l,k} \tag{20}$$

Starting from a known value at the solid base, the iterative process successively calculates the total solid masses until equilibrium is reached.

$$M_{S,i} = \sum_{k=1}^{N_k} \rho_s \phi'^{n+1}_{s,k} \Delta z^n_{l,k} \tag{21}$$

The concentration of a layer is determined using Eq. (19), and the new layer-bound cell height can be determined based on mass conservation (Eq. (18)) or the sum of the previously determined proportional individual heights as

$$\Delta z^{n+1}_i = \sum_{k=1}^{N_k} \Delta z^n_k \tag{22}$$

4.4. Results of the applied model

Since both samples G and J have almost the same grain size distribution and the approximated $\phi_{s,gel}$ and $\phi_{s,con}$ are almost the same for both samples, in this section the consolidation process is simulated only for sample G. The parameterized soil compressibility for the sample G is plotted using the obtained $\phi_{s,gel}$ and $\phi_{s,con}$ values in Fig. 13. In the permeability regime, the void ratio is relatively high and is primarily influenced by the permeability of the material. This regime corresponds to lower effective stresses where the material retains more

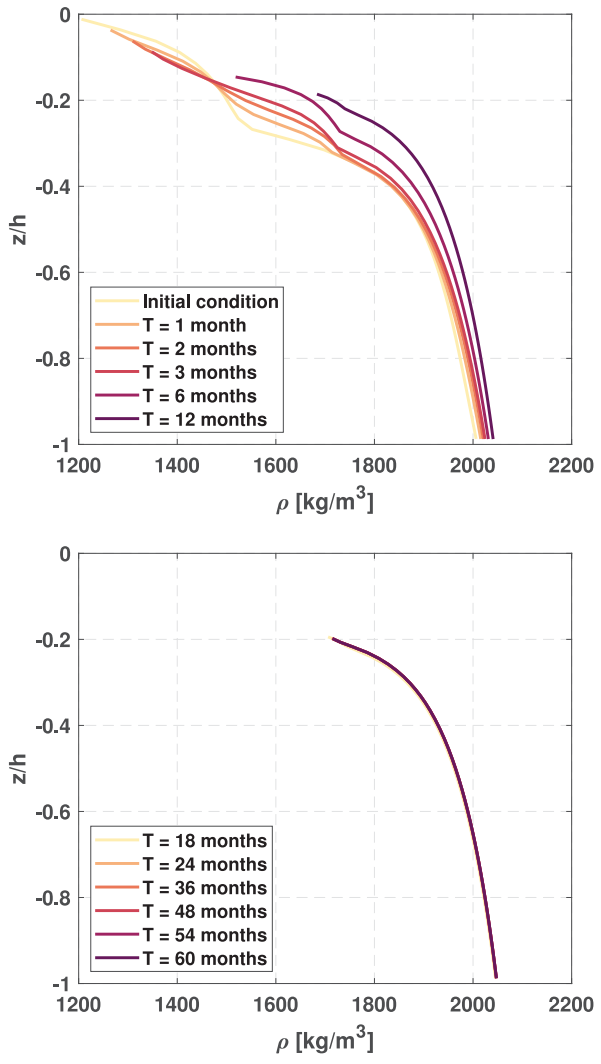

Fig. 14. Simulated density profiles based on the new proposed method and parameterization for the sample G.

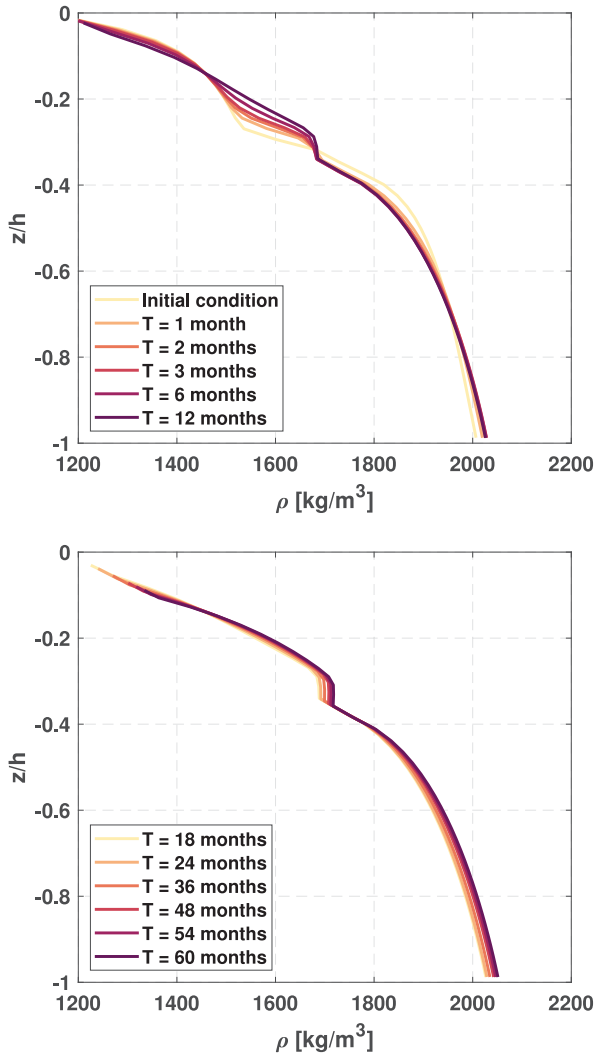

Fig. 15. Simulated density profiles based on the parameterization developed by Chauchat et al. (2013) for the sample G.

pore space. The effective stress regime corresponds to higher effective stresses where the void ratio is lower, indicating a denser packing of particles. In this regime, the void ratio is mainly controlled by the applied effective stress rather than the permeability of the material. As the effective stress increases, the particles become more densely packed and the void ratio decreases. Although it is necessary to perform a consolidation test to accurately calibrate this graph, Fig. 13 shows that the parameters used are within a physically realistic range. This is evident from the characteristic shapes and trends observed in the graph, which are consistent with the known behavior of soils and sedimentary materials under varying effective stress conditions.

Figs. 14 and 15 illustrate the evolution of bulk density ρ over relative height z/h at various times, from 1 month to 5 years. The analysis focuses on consolidation modeling based on the new proposed parameterization and the one proposed by Chauchat et al. (2013). The initial curve begins at the highest relative height ($z/h = 0$) and shows a gradual decrease in z/h as the density increases. This indicates initial consolidation as the sediment begins to settle. As can be seen from Fig. 14, there is a clear distinction between the upper layer representing the mud layer and the lower layer representing the cohesive bed. While the first layer settles faster and integrates with the cohesive layer, the consolidation process in the cohesive layer is slow. It should be noted that the first part is based on sedimentology and rheology considering

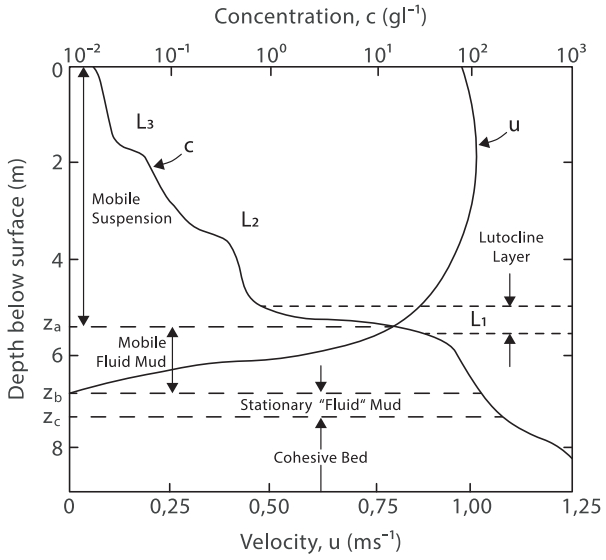

Fig. 16. Typical instantaneous concentration and velocity profiles in high concentration estuarine environment, modified from Ross and Mehta (1989).

the hindered settling rate (the permeability regime), the second part considers consolidation based on classical soil mechanics (the effective stress regime). In the absence of erosion or sedimentation (ignoring hydrodynamic conditions), after a long enough time, both layers are completely integrated, forming a single layer where only consolidation occurs. It can be seen that after almost 12 months the final consolidation process is almost achieved and changes thereafter are very slow. The inflection points observed in the new proposed model suggest a more realistic representation of sediment consolidation, accounting for the both regimes. This observation is logical, since the upper layer consists of newly deposited sediment, while the lower layer represents soil that has been in place for a longer period of time. In the case of estuaries, where the upper layer of mud can be eroded and deposited frequently, this parameterization may be appropriate.

Fig. 15 shows that the consolidation rate in the model presented by Chauchat et al. (2013) is almost the same for the whole layer, although initially a two-layer soil is considered at the beginning of the simulation. This model indicate an oversimplified model that fails to capture complex sediment behaviors influenced by environmental factors. If there is no erosion and sedimentation or changes in the upper layer, this parameterization may give reasonable results.

4.5. Discussion of findings

Fig. 16 shows a conceptual model of sediment concentration and velocity profiles during the transition from mobile suspension to consolidated bed in a sedimentary environment. With respect to the vertical structure of the concentration profile, three characteristic regions can be defined as an upper column mobile suspension layer, fluid mud layer and consolidated/cohesive bed. The typical largest layer, the mobile suspension which extends down to the lutocline layer, is not the focus of this study. After this layer, the lutocline layer gives way to the fluid mud layer where concentration is approximately at gelling point. The transition from stationary fluid mud to bed with porous solid properties is shown to occur at elevation z_c. Below this elevation, concentration becomes sufficiently high for soil structural development and non-zero effective stress (second consolidation phase) to occur (Ross and Mehta, 1989). According to this conceptual model, there is a smooth jump in the density profile entering the cohesive bed from the fluid mud layer. This jump and increase in concentration with depth can be clearly seen in the experimental studies performed and reported by Liu et al. (2017), who studied wave-induced seabed stratification. The thickness and form of mud layer under different sea conditions is discussed in detailed by Liu et al. (2022).

This makes sense because the flow velocity in the upper layer may be non-zero and therefore this layer may be more exposed to the frequent erosion and deposition process. As a result, it can be said that the characteristics of the upper layer, which is eroded and deposited more frequently, are quite different from the consolidated bed that has been there for a long time. The key differences are rooted in their rheological properties, with fluid mud behaving as a non-Newtonian fluid and consolidated beds behaving as solids with elastic (or plastic) deformation properties. The dispersed structure and dynamic behavior under stress of fluid mud contrasts with the solid matrix and rigidity of consolidated beds, which have higher density, strength, and low permeability.

Comparing the conceptual model shown in Fig. 16 with the results proves that the smooth transition model proposed by Chauchat et al. (2013) aligns with the general trend of increasing concentration but lacks detail in intermediate processes. The irregular transition obtained by the proposed model closely matches the conceptual figure's depiction of dynamic processes, explaining the observed inflection points and irregularities in sediment concentration and behavior.

5. Conclusion

This study established a theoretical framework for approximating the gelling concentration (c_{gel} or $\phi_{s,gel}$), as well as the concentration associated with the second consolidation phase (c_{con} or $\phi_{s,con}$), in sediment suspensions. Although the model is specifically tailored to parameterize soil consolidation processes in estuarine environments, it ensures that it remains relevant and useful for a wide range of applications and scenarios. By utilizing the interdisciplinary integration of rheology, colloidal science and sedimentology, the developed mathematical models provide robust predictions of the critical concentration at which sediments transition to a gel-like state and into the consolidation phase. Validation against empirical data underscores the models' performance in capturing the intricate interactions that dictate sediment behavior under diverse environmental conditions.

Applying the knowledge gained from the theoretical model, a more robust constitutive equation for the effective stress has been developed. While the previously proposed constitutive equations typically combine the permeability regime with the effective stress regime and use a single model for both regimes, the proposed model clearly accounts for both the permeability and effective stress regimes. This is achieved by taking into account the underlying physics of each regime. The new model shows inflection points indicating different consolidation rates, suggesting a more detailed representation of sediment behavior in the mud layer and cohesive bed. Analysis of the general conceptual model of sediment concentration and velocity profiles indicates that the new model better captures the physics of the consolidation process in estuaries by creating distinct layers during the first and second phase of consolidation.

CRediT authorship contribution statement

Keivan Kaveh: Writing – review & editing, Writing – original draft, Visualization, Methodology, Investigation, Formal analysis, Conceptualization. **Andreas Malcherek:** Validation, Supervision, Funding acquisition.

Declaration of competing interest

The authors declare that there are no potential conflicts of interests.

The author confirms that neither the co-author nor he has any personal or professional affiliations that could be perceived as having a potential conflict of interests regarding the research conducted in this paper.

Acknowledgments

Being part of the research project ELMOD, this research was supported by Bundesministerium für Bildung und Forschung (BMBF), Germany and executed by Jülich Forschungszentrum.

References

Camenen, B., van Bang, D.P., 2011. Modelling the settling of suspended sediments for concentrations close to the gelling concentration. Cont. Shelf Res. 31 (10), S106–S116.

Carman, P.C., 1939. Permeability of saturated sands, soils and clays. J. Agric. Sci. 29 (2), 262–273.

Casson, N., 1959. Rheology of disperse systems. Flow equation for pigment oil suspensions of the printing ink type. Rheol. Dispers. Syst. 84–102.

Chauchat, J., Guillou, S., Pham Van Bang, D., Dan Nguyen, K., 2013. Modelling sedimentation–consolidation in the framework of a one-dimensional two-phase flow model. J. Hydraul. Res. 51 (3), 293–305.

Cross, M.M., 1965. Rheology of non-Newtonian fluids: a new flow equation for pseudoplastic systems. J. Colloid Interface Sci. 20 (5), 417–437.

Dankers, P.J.T., Winterwerp, J.C., 2007. Hindered settling of mud flocs: Theory and validation. Cont. Shelf Res. 27 (14), 1893–1907.

Gibson, R.E., England, G.L., Hussey, M.J.L., 1967. The theory of one-dimensional consolidation of saturated clays: 1. finite non-linear consildation of thin homogeneous layers. Geotechnique 17 (3), 261–273.

Gibson, R.E., Schiffman, R.L., Cargill, K.W., 1981. The theory of one-dimensional consolidation of saturated clays. II. Finite nonlinear consolidation of thick homogeneous layers. Can. Geotech. J. 18 (2), 280–293.

Ichinose, N., Ura, H., 2020. Concentration dependence of the sol–gel phase behavior of agarose-water system observed by the optical bubble pressure tensiometry. Sci. Rep. 10 (1), 2620.
Kaveh, K., Malcherek, A., 2024a. Enhancing non-newtonian fluid modeling: a novel extension of the cross flow curve model. J. Hydro-environment Research 56, 17–27.
Kaveh, K., Malcherek, A., 2024b. On the global parameterization of a 1DV hydromorphodynamic model of estuaries, the case of the Ems estuary. Environ. Model. Softw. 106125.
Kozeny, J., 1927. Uber Kapillare Leitung Des Wassers Im Boden (Aufstieg, Versickerung Und Anwendung Die Bewässerung): Akademie Der Wissenschaften in Wien. Sitzungsberichte, Abt.
Kynch, G.J., 1952. A theory of sedimentation. Trans. Faraday Soc. 48, 166–176.
Liu, Y., Dai, C., Wang, K., Zhao, M., Zhao, G., Yang …, S., You, Q., 2016. New insights into the hydroquinone (HQ)–hexamethylenetetramine (HMTA) gel system for water shut-off treatment in high temperature reservoirs. J. Ind. Eng. Chem. 35, 20–28.
Liu, X., Jia, Y., Zheng, J., Wen, M., Shan, H., 2017. An experimental investigation of wave-induced sediment responses in a natural silty seabed: New insights into seabed stratification. Sedimentology 64 (2), 508–529.
Liu, X., Lu, Y., Yu, H., Ma, L., Li, X., Li ., W., Bian, C., 2022. In-situ observation of storm-induced wave-supported fluid mud occurrence in the subaqueous yellow river delta. J. Geophys. Res.: Oceans 127 (7), e2021JC018190.
Malkin, A.Y., Derkach, S.R., Kulichikhin, V.G., 2023. Rheology of gels and yielding liquids. Gels 9 (9), 715.
Merckelbach, L., 2000. Consolidation and strength evolution of soft mud layers.
Meshkati Shahmizadi, E., Wichman, B., Hansen, J., 2018. Pilot Kleirijperij. WP4.2.1 Voorbereidende Laboratoriumproeven. Deltares Rapport 11201344-000-ZKS-0006, EcoShape, Retrieved from https://www.ecoshape.org/nl/projecten/kleirijperij/.
Ross, M.A., Mehta, A.J., 1989. On the mechanics of lutoclines and fluid mud. J. Coast. Res. 51–62.
Schmidt, J., Malcherek, A., 2021. Using a holistic modeling approach to simulate mud-induced periodic stratification in hyper-turbid estuaries. Geophys. Res. Lett. 48 (20), e2021GL092798.
Te Slaa, S., He, Q., van Maren, D.S., Winterwerp, J.C., 2013. Sedimentation processes in silt-rich sediment systems. Ocean Dyn. 63, 399–421.
Thompson, D., Beasley, D.J., True, D.G., Lin, S.T., Briaud, J.L., Seelig, W.N., Jung, B., 2012. Handbook for marine geotechnical engineering.
Townsend, F.C., McVay, M.C., 1990. SOA: Large strain consolidation predictions. J. Geotech. Eng. 116 (2), 222–243.
Urmi, Z.A., Ansary, M.A., 2019. Interpretation of compressibility characteristics for coastal soil of Bangladesh. In: Proceedings on International Conference on Disaster Risk Management. Dhaka, Bangladesh.
Vermonden, T., Klumperman, B., 2015. The past, present and future of hydrogels. Eur. Polym. J. 72, 341–343.
Winterwerp, J.C., Van Kesteren, W.G., 2004. Introduction To the Physics of Cohesive Sediment Dynamics in the Marine Environment. Elsevier.
Zaccarelli, E., 2007. Colloidal gels: equilibrium and non-equilibrium routes. J. Phys.: Condens. Matter. 19 (32), 323101.
Zhou, Z., van der Wegen, M., Jagers, B., Coco, G., 2016. Modelling the role of self-weight consolidation on the morphodynamics of accretional mudflats. Environ. Model. Softw. 76, 167–181.